Structural and magnetic properties of layered $Sr_7Mn_4O_{15}$

Jaap F. Vente*
Cinvestav-IPN Unidad Mérida, Departamento de Física Aplicada, Carretera Ant. a Progreso km 6, Apartado Postal #73 Cordemex, Mérida, Yucatán, 97310, México

Konstantin V. Kamenev* and Dimitriy A. Sokolov
Department of Physics and Astronomy, The University of Edinburgh, JCMB, The Kings Buildings, Mayfield Road, Edinburgh EH9 3JZ, United Kingdom

(Received 15 December 2000; revised manuscript received 2 May 2001; published 1 November 2001)

The magnetic and structural properties of the layered manganite $Sr_7Mn_4O_{15}$ have been studied by powder neutron diffraction and magnetic susceptibility techniques between 5 and 300 K. The structure consists of pairs of face sharing MnO_6 octahedra to form Mn_2O_9 dimers. The description of the crystal structure has been improved by employing a model in which some of the Sr and O ions are statistically distributed over two different sites. Three different magnetic phases can be distinguished in the temperature region studied. Below ~75 K, the Mn^{4+} sublattice is antiferromagnetically ordered with an antiparallel alignment between all nearest-neighbor manganese ions. Between ~75 and ~150 K extensive quasi two-dimensional magnetic clusters are present. At temperatures above ~150 K, one can observe correlations related to intradimer spin pairing. Truly paramagnetic behavior is not observed at any temperature below 300 K.

DOI: 10.1103/PhysRevB.64.214403 PACS number(s): 75.50.Ee, 75.25.+z

INTRODUCTION

The magnetic properties of layered manganites have been studied extensively since the discovery of colossal magnetoresistance (CMR) in the $n=2$ Ruddlesden-Popper (RP) compound $Sr_{1.8}La_{1.2}Mn_2O_7$.[1] In this compound MnO_6 octahedra share corners to form layers which are two octahedra thick, separated by rock-salt-like SrO layers. The magnetic properties of these compounds depend strongly on the dopant level, and the size of the lanthanide ion. $Sr_{2.04}La_{0.96}Mn_2O_7$, e.g., orders antiferromagnetically at ~210 K,[2] but $Sr_{1.8}La_{1.2}Mn_2O_7$ (Ref. 1) is a ferromagnet below 126 K. However, an increase in the rare earth content in $Sr_2NdMn_2O_7$ does not result in a ferromagnetic phase, and antiferromagnetism is observed throughout the series.[3,4] Finally, if the lanthanide is sufficiently small, such as Ho or Y, a spin-glass-like state is observed.[5] CMR has been observed in mixed valence $n=2$ RP phases that contain rare earth cations larger than Sm, but was not found when smaller R ions are present.[6,7] The average formal valence of these Mn^{3+}/Mn^{4+} containing compounds also influences the CMR, and a value of about +3.4 appears to be optimal. However, CMR is not limited to mixed valence compounds, but it is also found in some compounds in which manganese has a formal valence very close to +4, e.g., the pyrochlore $Tl_2Mn_2O_7$,[8] and the $n=3$ RP phase $Ca_4Mn_3O_{10}$.[9]

All the compounds mentioned above have one important structural feature in common: MnO_6 octahedra share only corners to form a two-dimensional (2D) or 3D network. Currently, we are investigating the possible presence of magnetoresistance in compounds in which the MnO_6 octahedra share not only corners but also faces. As a result the Mn-O-Mn super exchange pathways are not restricted to 180° interactions only, but it allows for competition with 90° interactions.[10] To our knowledge, no mixed valence manganites in which octahedra share faces are reported in the literature. Doping of $4H$ $SrMnO_3$ and $2H$ $BaMnO_3$ with a lanthanide is feasible but results in the formation of a distorted $3C$ perovskite.[11] We therefore aim to dope more complex phases that may not transform as easily into a different structure. The first potential host lattice we have identified is that of $Sr_7Mn_4O_{15}$. The structure of this compound has been described before[12,13] and is presented in Fig. 1. Manganese is present as Mn^{4+} and is located solely in pairs of face sharing octahedra which are similar to those found in $4H$ $SrMnO_3$.[14] The Mn_2O_9 groups are linked to six analogous groups in $SrMnO_3$, but only to three in $Sr_7Mn_4O_{15}$. Two crystallographically distinct Mn cations can be distinguished in this structure. Mn(1) shares two oxide ions with two neighboring dimers, whereas Mn(2) shares only one oxide ion with a neighboring dimer. The Mn(1)-O-Mn(2) coupling creates columns which are joined by Mn(1)-O-Mn(1) linkages every ~10.3 Å to form layers. In this way a 2D compound with a strong in-plane anisotropy is formed. The structure can thus be considered as a combination of the $n=1$RP phase of Sr_2MnO_4 (Ref. 15) and the $4H$ perovskite $SrMnO_3$:[14] a single layer compound with Mn_2O_9 dimers as principle building blocks. The structure of $Sr_7Mn_4O_{15}$ is fairly flexible and up to ~30% of the Sr ions can be replaced by Ba and Ca ions, without any significant change in the crystal structure.[12] The application of chemical pressure does cause the cell parameters to change in an anisotropic fashion, thus reflecting the cation ordering that occurs between the different alkaline earth metal ions.[12]

Up to date, little information is available on the electronic and magnetic properties of $Sr_7Mn_4O_{15}$. Only the high-temperature behavior of the electronic conductivity has been published, reporting that the material is a highly resistive insulator.[16] Due to this very high resistivity, $Sr_7Mn_4O_{15}$ is

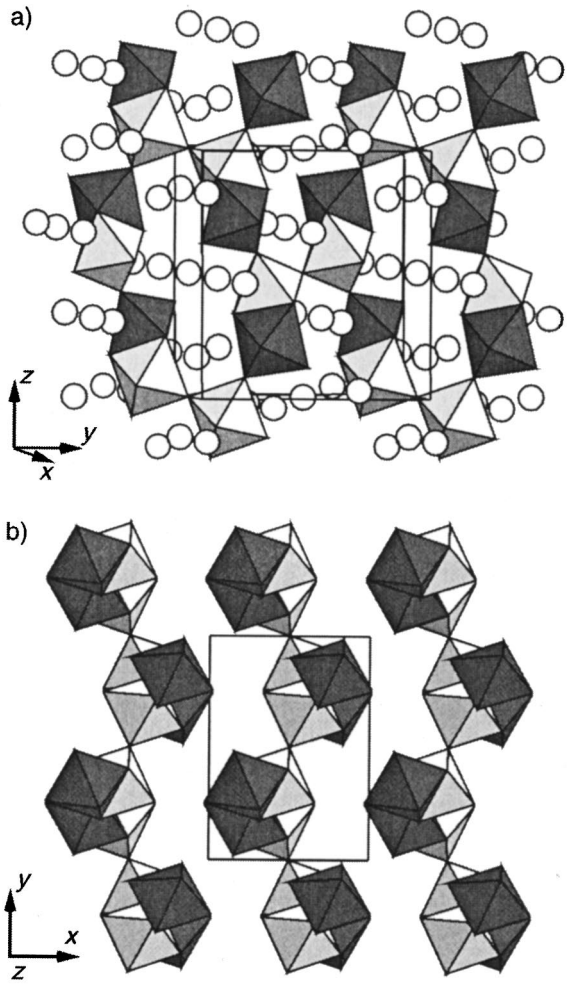

FIG. 1. Two views of the crystal structure of $Sr_7Mn_4O_{15}$, Mn(1) (light) and Mn(2) (dark) octahedra are shown, and Sr is shown as circles. (a) emphases the linking within planes, while (b) shows the columns and stacking of the planes.

unlikely to show magnetoresistance, but we hope to be able to reduce the resistivity by doping with a lanthanide. In the current report, we present and discuss the results of an extensive study of the unique structural and the intriguing magnetic properties of novel $Sr_7Mn_4O_{15}$ in which manganese is found as Mn^{4+} only, using variable temperature neutron diffraction and ac/dc magnetization measurements. Our results and conclusions should be of special interest as a test system to theoreticians who develop models of magnetic interactions in manganese oxides.

EXPERIMENTAL

The synthesis of an 8 g polycrystalline sample of $Sr_7Mn_4O_{15}$ was started by heating a stoichiometric mixture of high purity $SrCO_3$ and MnO_2 in an alumina crucible in air at 800 °C (1 d). Subsequently, the mixture was reground and pelletized and fired at 1000 °C (1 d), 1200 °C (1 d), 1300 °C (10 d) with further grindings. After the last firing the sample was furnace cooled to 1000 °C and subsequently air quenched to room temperature. X-ray data (XRD, Cu$K\alpha_{1+2}$) were recorded using a Siemens D5000 diffractometer operating at room temperature in Bragg-Brentano geometry over the angular range $5° \leqslant 2\theta \leqslant 80°$ in steps of $0.02°2\theta$. This limited angular range was used because no peaks with an appreciable intensity above the background level were observed at higher angles. Variable temperature time-of-flight powder neutron diffraction data (PND) were obtained on the instrument Osiris at the ISIS facility, Rutherford Appleton Laboratory. Data were collected at ~20 different temperatures between 5 and 290 K using an orange ILL cryostat, in the *d*-spacing range $0.96\,\text{Å} \leqslant d \leqslant 7.11\,\text{Å}$ on the sample contained in a cylindrical vanadium can. The data were normalized for *Q* dependence of the primary beam and corrected for detector efficiency and empty sample holder effects. The widths of the Bragg reflections of $Sr_7Mn_4O_{15}$ proved to be comparable with those of Si, this together with the high degree of peak overlap at small *d* spacing made us decide to use a relatively small part of the detector bank (10%) to obtain the highest resolution possible at the cost of reduced counter statistics.

All neutron diffraction data were analyzed by the Rietveld method,[17] as implemented in the GSAS program suite.[18] Scattering lengths and the magnetic form factor for Mn^{4+} were used as provided by this software package. The background levels were modelled using a power series in *Q* [Eq. (4) in the GSAS package, six parameters] to account for the increase in the background with *Q*. The peak shape was described using a convolution of the Ikeda-Carpenter and pseudo-Voigt functions after David[19] (three refineable parameters). Also a wavelength-dependent absorption correction according to an empirical formula after Hewat[20] was included.

Direct current magnetization measurements were performed on a Quantum Design MPMS superconducting quantum interference device magnetometer in the temperature range $5\,\text{K} \leqslant T \leqslant 300\,\text{K}$, in magnetic fields of 100 and 1000 G. The data were collected on warming after cooling the sample in zero field (ZFC) and after cooling in the measuring field (FC). The same sequence of measurements was applied for the other members of the series $Sr_{7-x}(Ca/Ba)_xMn_4O_{15}$.[21] Hysteresis loops in the range $-2\,\text{kG} \leqslant H \leqslant 2\,\text{kG}$ were recorded after cooling in a field of 2 kG at selected temperatures. The ac susceptibility was measured in the temperature range $5\,\text{K} \leqslant T \leqslant 300\,\text{K}$, in dc bias fields of zero and 1 kG with the amplitude of the oscillating field of 1 and 2 G at 1, 10, and 113 Hz.

Several attempts were made to measure the conductivity using a standard four probe dc technique on pellets $Sr_7Mn_4O_{15}$. The resistance of the pellets proved to be too high to be measured with our equipment ($>1\,\text{M}\Omega$), over the full temperature range used ($5\,\text{K} \leqslant T \leqslant 350\,\text{K}$), and we were unable to establish the possible presence of magnetoresistance.

RESULTS

The XRD pattern of our final product was identical to data collected previously on other samples,[12,13] and the PND col-

TABLE I. Structural parameters of $Sr_7Mn_4O_{15}$ at 290 K. Space group $P2_1/c$; $a=6.81825(9)$, $b=9.6228(1)$, $c=10.3801(1)$ Å, $\beta=91.8771(9)°$, $V=680.68(1)$ Å^3, all atoms at $4e$. For all Sr $U_{iso}=0.007(1)$ Å^2, for all Mn $U_{iso}=0.001(1)$ Å^2, for all O $U_{iso}=0.012(7)$. Agreement indices: $R_{wp}=7.66\%$, $R_p=9.95\%$, $DWd=1.15$, $\chi_{red^2}=1.91$ for 59 variables.

Atom	*x*	*y*	*z*
Sr(1)	0.9974(9)	0.1861(6)	0.4621(5)
Sr(2)	0.351(1)	0.1540(5)	0.1936(5)
Sr(3)[a]	0.500(3)	0.021(1)	0.510(1)
Sr(4)	0.1828(9)	−0.019(5)	0.8345(7)
Mn(1)	0.589(1)	0.165(1)	0.9246(9)
Mn(2)	0.781(1)	0.1701(9)	0.7199(8)
O(1)	0.512(1)	0.1038(7)	0.7525(7)
O(2)	0.682(1)	0.1758(7)	0.3389(7)
O(3)	0.331(1)	0.2528(8)	0.9532(7)
O(4)	0.839(1)	0.0845(7)	0.8852(7)
O(5)	0.682(1)	0.2220(7)	0.0839(8)
O(6)[a]	0.503(3)	0.005(3)	−0.024(2)
O(7)	0.839(1)	0.0148(7)	0.6221(6)
O(8)	0.026(1)	0.2492(6)	0.7110(7)

[a]Fractional occupancy of Sr(3) and O(6) is 0.5.

lected at 290 K was consistent with our simulations based on the published crystal structure data[13] but the structural refinement using the 29 K PND data resulted in a nonsatisfactory fit. Inspection of the difference Fourier map, indicated that Sr(3) and O(6) ions were actually displaced from their positions. In addition, their individual displacement parameters appeared to be abnormally high. A significant improvement of the fit was achieved when these ions were allowed to move from their ideal position to a general position with a fractional occupancy of 0.5, thus keeping the composition unchanged. We applied constraints to keep the displacement factor of each type of ion the same. In addition it proved to be necessary to include a parameter describing absorption effects. At this point, the refinement rendered unstable due to correlation effects between the scale factor, the absorption correction and the displacement factors. We, therefore, fixed the absorption at such a value that reasonable displacement factors were found. This fixed value for the absorption was subsequently used in all the Rietveld refinements using PND collected at the various temperatures. The refined structural parameters of $Sr_7Mn_4O_{15}$ at 290 K are presented in Table I, and a list of bond distances and selected bond angles is given in Table II. The diffraction profiles are shown in Fig. 2.

TABLE II. Bond lengths (Å) and bond angles (deg) in $Sr_7Mn_4O_{15}$ at 290 K. Mean Sr(1)-O (8 coordination): 2.55(12) Å, Sr(2)-O (10 coordination): 2.67(13) Å, Sr(3)-O (10 coordination): 2.77(22) Å, Sr(4)-O (10 coordination): 2.74(18) Å, Mn(1)-O: 1.90(8) Å; mean Mn(2)-O: 1.92(8) Å.

Sr(1)-O(2)	2.467(9)	Sr(2)-O(1)	2.702(9)	Sr(3)-O(1)	2.64(2)
Sr(1)-O(3)	2.36(1)		2.639(9)		2.97(2)
Sr(1)-O(4)	2.571(9)	Sr(2)-O(2)	2.680(9)	Sr(3)-O(2)	2.66(2)
Sr(1)-O(5)	2.678(9)	Sr(2)-O(3)	2.85(1)		2.77(2)
Sr(1)-O(7)	2.602(9)		2.67(1)	Sr(3)-O(3)	2.84(2)
	2.412(9)	Sr(2)-O(4)	2.571(9)		2.52(2)
Sr(1)-O(8)	2.65(1)	Sr(2)-O(5)	2.64(1)	Sr(3)-O(5)	2.86(2)
	2.69(1)	Sr(2)-O(6)[a]	2.90(2)		3.26(1)
			2.55(2)	Sr(3)-O(7)	2.55(2)
Sr(4)-O(1)	2.63(1)	Sr(2)-O(7)	2.853(9)		2.67(2)
Sr(4)-O(2)	2.65(1)	Sr(2)-O(8)	2.42(1)		
Sr(4)-O(3)	2.910(9)				
Sr(4)-O(4)	2.554(9)	Mn(1)-O(1)	1.94(1)	Mn(2)-O(1)	1.98(2)
	3.02(1)	Mn(1)-O(2)	1.88(1)	Mn(2)-O(2)	2.06(1)
Sr(4)-O(5)	2.449(9)	Mn(1)-O(3)	1.98(1)	Mn(2)-O(4)	1.93(1)
Sr(4)-O(6)	2.59(2)	Mn(1)-O(4)	1.93(1)	Mn(2)-O(5)	1.86(1)
	2.86(2)	Mn(1)-O(5)	1.83(1)	Mn(2)-O(7)	1.86(1)
Sr(4)-O(8)	2.922(9)	Mn(1)-O(6)[a]	1.74(3)	Mn(2)-O(8)	1.84(1)
	2.818(9)		2.05(2)		
Sr(3)-Sr(3)	0.45(3)	Mn(1)-Mn(1)	3.77(2)	O(6)-O(6)	0.53(3)
		Mn(1)-Mn(2)	2.53(1)		
			3.65(1)		
O(3)-O(5)	2.72(1)	O(1)-O(2)	2.56(1)	O(5)-O(7)	2.77(1)
O(3)-O(6)	2.66(2)	O(1)-O(4)	2.59(1)	O(5)-O(8)	2.66(1)
O(5)-O(6)	2.58(3)	O(2)-O(4)	2.58(9)	O(7)-O(8)	2.73(1)
	2.65(3)				
O(2)-Mn(1)-O(5)		94.2(6)	Mn(1)-O(5)-Mn(2)		162.9(7)
Mn(1)-O(2)-Mn(2)		79.7(4)	Mn(1)-O(6)-Mn(1)		167(1)

[a]50% occurrence.

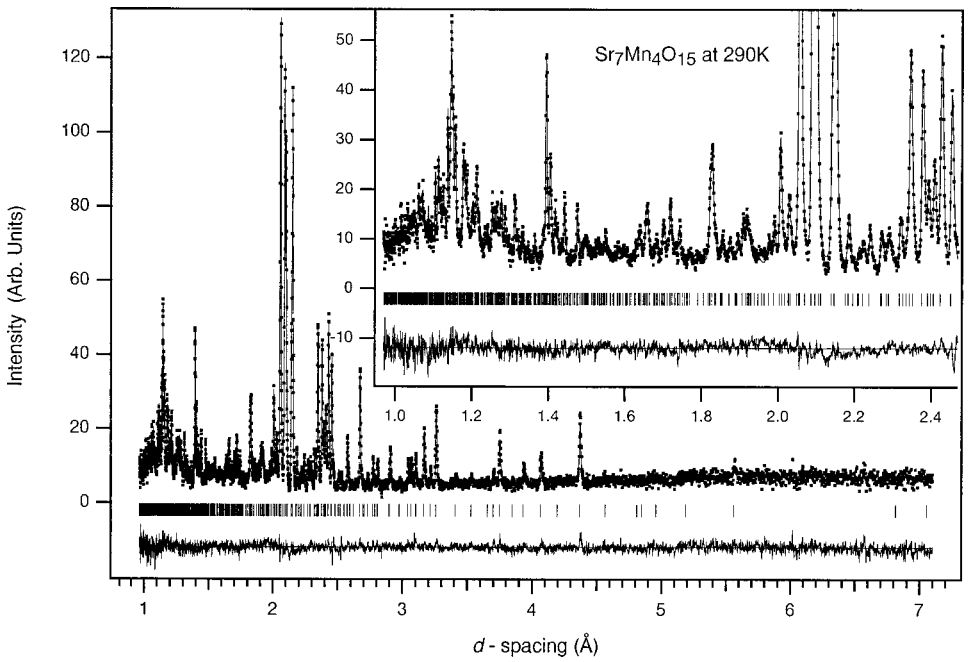

FIG. 2. Observed (dots), calculated (top line), and difference (bottom line) PND profiles of $Sr_7Mn_4O_{15}$ at 290 K. Reflection positions are marked.

The dc molar susceptibility of $Sr_7Mn_4O_{15}$ is plotted as afunction of temperature in Fig. 3(a). Attempts to model the high-temperature region using a Curie-Weiss law resulted in nonsensical values ($\mu_{\text{eff}}=4.47\mu_B$ per Mn, $\theta=-490$ K). It immediately became clear that interatomic magnetic interactions are significant throughout the measured temperature range. A clear maximum is observed at ~90 K, which might be indicative of the onset of cooperative effects. The rather large width of this maximum, however, suggests that this is not a transition from a high temperature paramagnetic state to a low temperature 3D-magnetically ordered state. The slight difference between the ZFC and FC susceptibilities at even lower temperatures, along with the small displacement of the center of the FC hysteresis loop at 5 K away from the origin [Fig. 3(b)], is characteristic for spin-glass-like behavior. The magnetic susceptibility of the compounds $Sr_{7-x}(Ca/Ba)_xMn_4O_{15}$ did not show a significant dependency on the calcium and/or barium content.[21] In order to get a more detailed insight in the spin dynamics of $Sr_7Mn_4O_{15}$, we measured the ac susceptibility as shown in Fig. 4(a). The plot of χ_{ac} vs T is rather featureless, and does

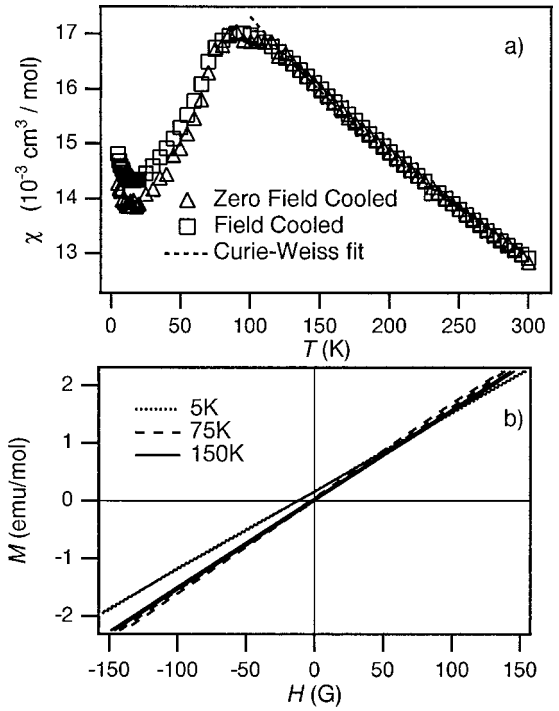

FIG. 3. The ZFC and FC molar magnetic susceptibilities measured in a dc field of 100 G (a), and the central part of the hysteresis loops after cooling the sample in 2 kG (b).

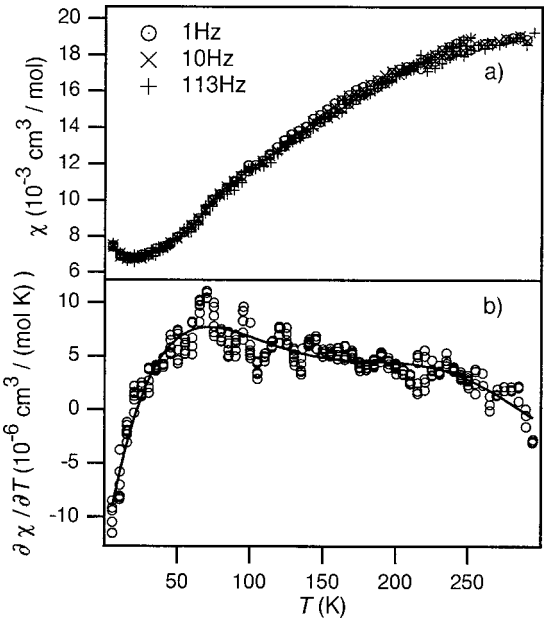

FIG. 4. The ac magnetic susceptibility as a function of temperature at three different frequencies measured at zero bias field with an amplitude of 2 G (a), and the partial differential $\partial\chi_{\text{ac}}/\partial T$(b).

not show any frequency dependency. The slight upturn at temperatures below ~20 K is also observed in the dc susceptibility of all compounds measured and appears to be an intrinsic property of the $Sr_{7-x}(Ca/Ba)_xMn_4O_{15}$ series, rather than the result of a slight impurity.[21] The differential $\partial\chi_{ac}/\partial T$ [Fig. 4(b)] was fitted to four-term polynomial which shows a weak maximum at ~70 K rendering the transition from concave to convex behavior of χ_{ac}. The combined analysis of the dc and ac magnetic susceptibilities does not provide enough information about neither the presence or absence of a long-range magnetic order, nor about a possible transition temperature.

To resolve the ambiguity in the magnetic susceptibility measurements we collected PND patterns at various temperatures between 5 and 290 K. In comparison with the data collected at 290 K, the data set collected at 5 K contained a considerable number of additional Bragg peaks at d values larger than 3 Å (Fig. 5), which we assumed to be magnetic in origin. All the additional peaks could be indexed using the crystallographic cell and no cell multiplication was required. The presence of the {1 0 0} and {0 0 2} reflections indicated that the moments are directed along the y direction. Several models were tested, and the one in which each manganese couples antiferromagnetically to the nearest neighbor (Fig. 6) provided the best fit to the observed data. The ordered moment refined to a value of 2.83(2) μ_B per Mn. We cannot be sure about the absolute value of the quantity, due to the correlation effects discussed earlier in this paper. However, we are confident that the values are self consistent and that the comparison between different temperatures is valid. We will come back to this in the discussion. No crystallographic phase transition was observed and the cell parameters at 5 K refined to the following values: $a=6.80928(8)$, $b=9.5999(1)$, $c=10.3492(1)$ Å, and $\beta=91.922(1)°$. We followed the development of the intensities of the magnetic Bragg reflections with increasing temperature and found that

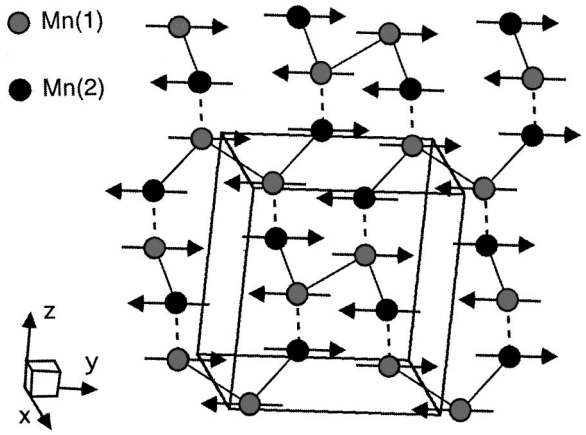

FIG. 6. The magnetic structure of $Sr_7Mn_4O_{15}$.

they decrease to the noise level at ~75 K, thus providing an estimate for the Néel temperature (T_N). The temperature dependence of the magnetic moments per Mn site is depicted in Fig. 7(a) for $T \leqslant 75$ K. We show in Fig. 7(b) the average background level in the d-spacing range $4.6\,\text{Å} \leqslant d \leqslant 6.6\,\text{Å}$. We took care not to include any intensity originating from allowed Bragg reflections, and we thus excluded the following parts: $4.86\,\text{Å} \leqslant d \leqslant 4.98\,\text{Å}$, $5.09\,\text{Å} \leqslant d \leqslant 5.22\,\text{Å}$, and $5.48\,\text{Å} \leqslant d \leqslant 5.63\,\text{Å}$, where the {1 1 −1}, {0 0 2}, and {1 1 0} reflections are located, respectively. There is a general trend of an increasing background level with increasing temperature, which can be attributed to the influence of phonons. However superimposed on this trend, is a broad but clearly visible peak present with its maximum centred at ~85 K, suggesting the presence of magnons resulting in regions with correlated spins just above T_N. The presence of this increased background level is illustrated in Fig. 7(c), where we depict the background level (I_b) at 5 and 85 K relative to

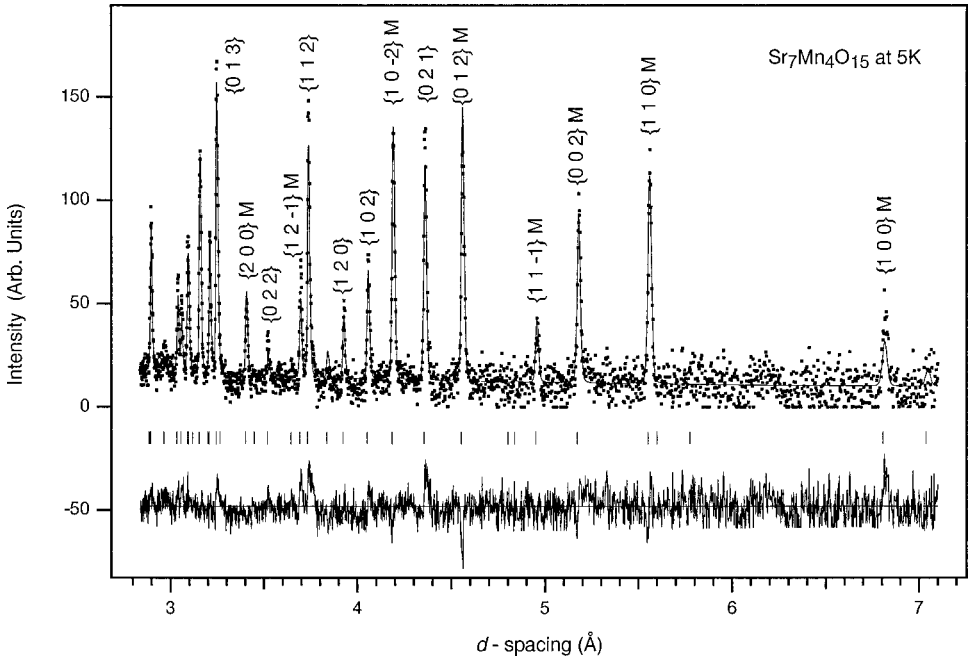

FIG. 5. Observed (dots), calculated (top line), and difference (bottom line) PND profiles of $Sr_7Mn_4O_{15}$ at 5 K. Reflection positions where nuclear and/or magnetic Bragg intensities may be observed are marked. The main peaks are indexed and those with a predominant magnetic contribution are labeled (M).

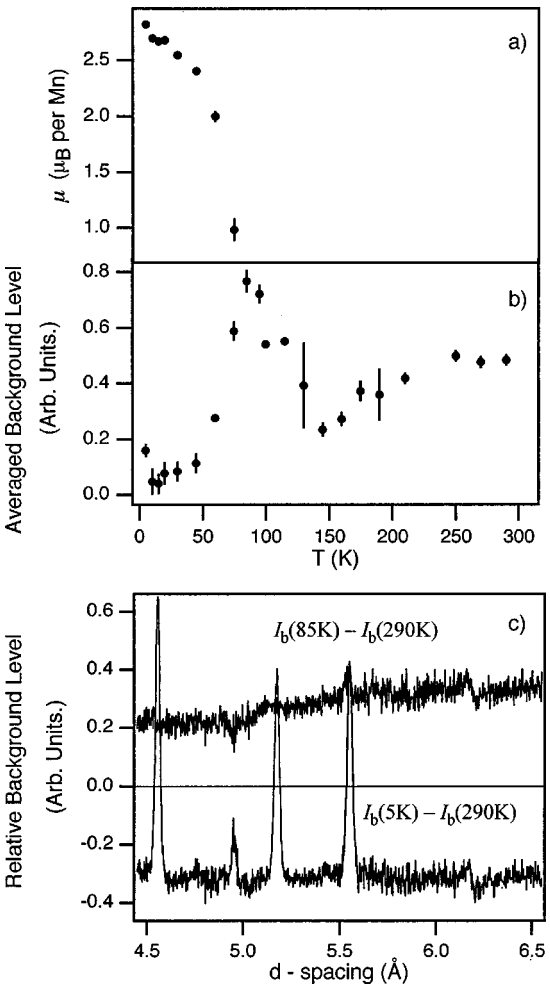

FIG. 7. (a) The ordered magnetic moment on the manganese sites; (b) the average background level as a function of temperature; (c) the relative background level at 5 (top) and 85 K (bottom) calculated according to $I_b(5\text{ K}) - I_b(290\text{ K})$ and $I_b(85\text{ K}) - I_b(290\text{ K})$, respectively.

that at 290 K. The horizontal zero line represents the background level at 290 K.

To study the relative influence of the different superexchange interaction pathways as well as the possible presence of spin pairing, we have determined the crystallographic properties as a function of temperature. The relative cell parameters ($l/l_{290\text{K}}$, Fig. 8) change smoothly with temperature, and the *a* axis showing the smallest reduction on cooling and the *c* axis the largest (0.15 and 0.3 % respectively). Little variation is observed below 50 K; and there are no indications of discontinuities. The monoclinic angle (β) increases very slightly (0.05%) with decreasing temperature. In Fig. 9 we depict the three different characteristic Mn-Mn distances present in $Sr_7Mn_4O_{15}$ as a function of temperature. In contrast with the smooth changes of the cell parameters, clear discontinuities can be seen, despite the relatively large error bars in this graph. Above 130 K, the intradimer Mn(1)-Mn(2) distance is roughly constant at ~2.54 Å, but it becomes somewhat smaller in the interval $75\text{ K} \leqslant T \leqslant 115\text{ K}$ (~2.51 Å). Surprisingly, on further cooling the distance increases again and becomes almost constant, at 2.58 Å, T

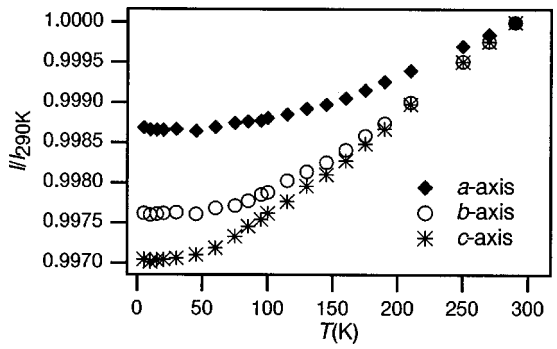

FIG. 8. The relative cell parameters, for $l = a$, b, and c, as a function of temperature, the estimated standard deviation is considerable smaller than the size of the marker.

<30 K. The behavior of the interdimer Mn(1)-Mn(2) bond length is very different. Above 85 K, this distance is constant within the error bars at ~3.64 Å. On further cooling, it decreases to ~3.58 Å below 30 K. This shortening might be related with exchange striction effects[22] caused by the onset of long range magnetic ordering. The interdimer Mn(1)-Mn(1) distance is not very well established, but the values for $T \leqslant 30$ K appear to be larger than those at higher temperatures. The Mn(1)-O(1) bond length and O(2)-Mn(1)-O(5) bond angle are presented in Fig. 10. O(1) {O(2)} is located

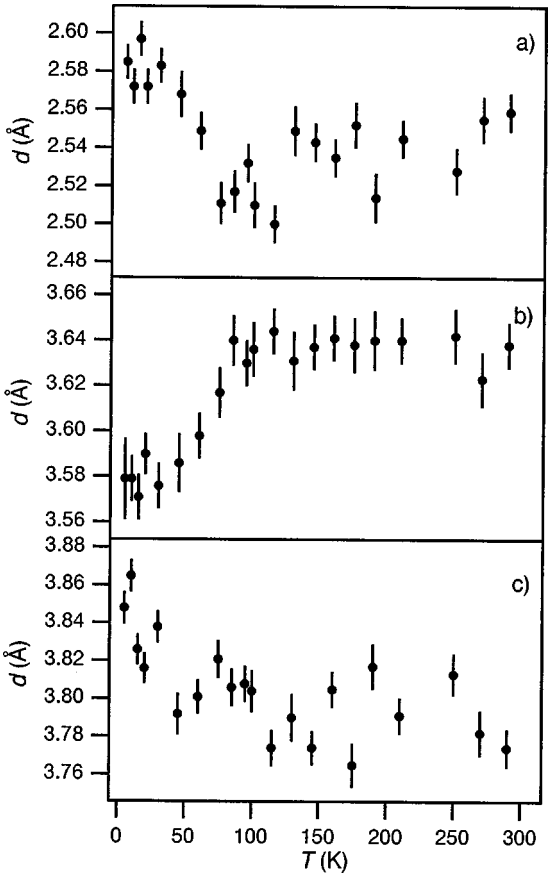

FIG. 9. The intradimer Mn(1)-Mn(2) (a), the interdimer Mn(1)-Mn(2) (b), and the interdimer Mn(1)-Mn(1) (c) distance as a function of temperature.

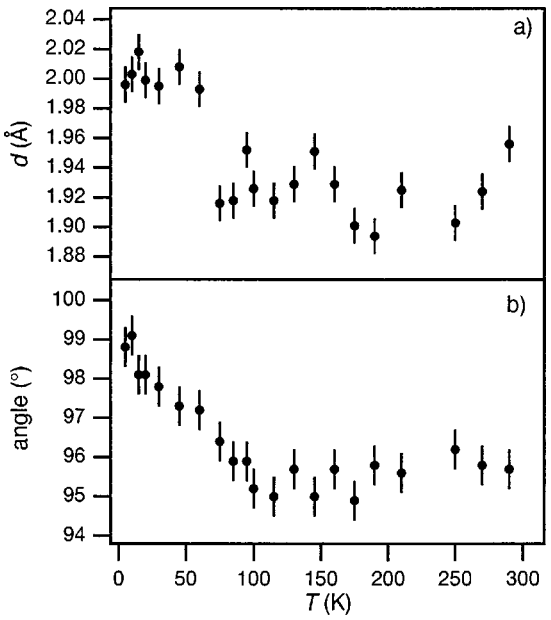

FIG. 10. The Mn(1)-O(1) bond length (a) and the O(2)-Mn(1)-O(5) bond angle (b) as a function of temperature.

opposite from the O(5){O(6)}, the oxide ion that connects Mn(1) {Mn(1)} with Mn(2) {Mn(1)}. Both O(1) and O(2), together with O(4), are found in the central plane of the Mn_2O_9 dimers. On cooling the Mn(1)-O(1) distance increases at ~75 K from ~1.92 to ~2.00 Å. The O(2)-Mn(1)-O(5) bond angle is constant above 85 K (~95.5°), but increases steadily below this temperature reaching a maximum of ~99.0° at 5 K. Similar relations could not be found for Mn(2). All these data seem to indicate that Mn(1) has a much higher positional freedom than Mn(2), and that the main contribution to the chances of the Mn(1)-Mn(2) distances is achieved through a movement of Mn(1).

DISCUSSION

The structural chemistry of $Sr_7Mn_4O_{15}$ as determined by us differs from that reported before by Kriegel.[13] The formal valence of manganese is not reduced from the expected value of 4, as can be concluded from the bond lengths listed in Table II. We do not observe the presence of a Jahn-Teller distortion which might have been present for the d^4-ion Mn^{3+}. In addition the average bond lengths (~1.91 Å), as well as the spread, are consistent with that found in other Mn^{4+} containing compounds such as $Ca_4Mn_3O_{10}$,[23] $Ca_{2-x}Sr_xMnO_4$,[24] $SrMnO_3$,[14] $Sr_4Mn_3O_{10}$,[25] and $BaMnO_3$.[26] Our cell parameters are in perfect agreement with those reported before.[12,13] In contrast with earlier determinations we do observe that two atoms which were located on a high symmetry site by Kriegel[13] are actually evenly spread over two general sites with an occupancy of 0.5. It is of course possible that our powdered sample is genuinely different from the single crystal used by Kriegel, but there are reasons to believe otherwise. First, the anisotropic displacement factors in the original paper provide a hint that Sr(3) is not located on the high symmetry site, as U_{22} of this ion is significantly larger than U_{11} and U_{33}. The relative scattering power of O compared with Sr and Mn is much higher in a PND experiment than in an XRD experiment, and it is for this reason very well possible that Kriegel[13] did not observe this oxide disorder.[13] The origin of this positional disorder is not very obvious. The Mn(1)-Mn(1) distance via O(6) does not appear to be too short to require a buckling of the Mn(1)-O(6)-Mn(1) bond angle. On the other hand though, the displacement of the Sr cation appears to result in a slightly more favorable bond valence sum.[27] The O-O bond lengths are consistent with other oxides. Those in the face separating the two MnO_6 octahedra (~2.57 Å) are significantly shorter than those at the edges (~2.66 and ~2.72 Å), providing enough shielding to compensate for the repulsive forces between the two positively charged Mn ions located at a short distance from each other.

The variation of the cell parameters with temperature is anisotropic. The *a* parameter shows a much smaller change compared to the *b* and *c* parameters (Fig. 8), indicating that the interplane distance is much less affected by the temperature than the intraplane distances. The temperature dependence for all the cell parameters is smooth without any noticeable features. This is remarkable given the pronounced temperature dependence of some of the bond distances as will be discussed below. The structure is apparently flexible enough to absorb these changes, by adjusting other bond distances.

However, the main topic of this paper is the rather intriguing magnetic properties of the title compound $Sr_7Mn_4O_{15}$. When we first observed the maximum in χ_{dc} vs T at ~100 K (Fig. 3), we interpreted this as the transition from a paramagnetic state to an antiferromagnetically ordered state. However, this maximum appeared to be too broad for a conventional Néel temperature. In addition, the non-Curie-Weiss behavior of the high-temperature part made us doubt the interpretation of the high-temperature region. Finally, the fact that all compounds $Sr_{7-x}(Ca/Ba)_xMn_4O_{15}$ showed the same behavior within the errors,[21] made us question the explanation of the low-temperature region. The variable temperature neutron diffraction experiments prove unambiguously that $Sr_7Mn_4O_{15}$ shows long-range antiferromagnetic order below ~75 K, and thus that the maximum at 90 K on the dc susceptibility curve is not related to the Néel temperature. The magnetic structure is consistent with that commonly found in magnetically ordered manganites with a hexagonal perovskite related structure. In such compounds, octahedra share faces and the moments are normally aligned perpendicular to the hexagonal axis, and thus parallel with the face which the two-paired octahedra have in common.[26,28] In addition, antiferromagnetic coupling is present between all nearest-neighbor transition metal ions. These characteristics are also found in the current compound, and the magnetic moments are fully compensated within the layers. The relatively low structural symmetry of $Sr_7Mn_4O_{15}$ allows us to determine the exact direction of the magnetic moment. The moments are aligned within the layers and are parallel with the *b* axis. Magnetic coupling between the layers is achieved through multiple AFM Mn(2)-O-Sr-O-Mn(2) superexchange pathways with a Mn-Mn separation of ~5.7 Å. The observed

magnetic moment of $2.83(2)\mu_B$ is somewhat lower than the theoretical value for Mn^{4+}, $gS=3\mu_B$, but higher than the commonly observed value of about $2.3\mu_B$.[23,28] This shows that although we can not be sure about the absolute value of this quantity due to the correlations in the refinement, the corrections we have applied are reasonable and that our interpretations are valid.

The neutron diffraction patterns collected between 60 and 150 K show further an enhanced background level at a relatively large *d* spacing. We assign this to the presence of extensive short-range magnetic correlations, with a clusterlike behavior. The alternative description of increased incoherent scattering is inconsistent with the fact that the effect is only observed over a very limited temperature range. These magnetic clusters are likely to have a two-dimensional character as the largest nearest-neighbor interdimer Mn-Mn distance is ~3.7 Å and the shortest interlayer Mn-Mn distance is ~5.7 Å. Not only the PND experiments hint at the presence of clusters but also the magnetic susceptibility measurements. The presence of a small but significant divergence between the FC and ZFC data below T_N indicate that not all the magnetic moments are totally compensated. The small values of the susceptibility combined with the fact that the center of the FC hysteresis loop at 5 K is not centered around the origin rule out a minor spin canting, and indicate spin or cluster-glass-like behavior.

One of the short-range coupling mechanisms to look at, is the spin pairing as has been observed between the spins of two Mn^{4+} ions in the Mn_2O_9 dimers of $SrMnO_3$.[14] Such a spin pairing is unlikely to cause the high background feature in the PND as it is only effective over very short distances (~2.5 Å). Our data thus indicate that interdimer coupling is present below ~150 K. Above this temperature the contribution to the background from the magnetic fluctuations disappears. The only type of short range correlations which might still be present above 150 K is a spin pairing of the type observed below 350 K in $SrMnO_3$. However, the dc susceptibility above T_N of $SrMnO_3$ and $Sr_7Mn_4O_{15}$ behave very different. The dc susceptibility of $SrMnO_3$ above T_N increases with increasing *T*, similarly to the behavior of a polycrystalline antiferromagnetically ordered compound. Contrary to this, χ_{dc} of $Sr_7Mn_4O_{15}$ decreases with increasing *T* above 120 K (and thus above T_N), analogous to a paramagnet. The dc magnetic susceptibility data thus seem to indicate that no spin pairing is present in $Sr_7Mn_4O_{15}$. The structural data, on the other hand, show a very similar intradimer Mn-Mn distances for $Sr_7Mn_4O_{15}$ and $SrMnO_3$ (2.53 and 2.50 Å, respectively, at ~290 K) and thus imply that such a coupling scheme could indeed be possible.

In the discussion on the possible spin pairing in $Sr_7Mn_4O_{15}$ it is important to remember that the MnO_6 octahedra in $Sr_7Mn_4O_{15}$ are very irregular and that it is therefore not straight forward to predict how the different energy levels of *d* orbitals are arranged. If the octahedra were perfectly regular, the structure would consist exclusively of Mn^{4+} with a half filled t_{2g} triplet and an empty e_g doublet. When the octahedron is elongated, the t_{2g} orbital splits into an e_g doublet and a b_{2g} singlet which is higher in energy. We suggest now that the spin pairing continuously diminishes over a large temperature range and that it is still present at 300 K, the highest temperature used in our studies. We will now show how this model can account for the apparent contradiction between the negative $\partial\chi_{dc}/\partial T$ and the positive $\partial\chi_{ac}/\partial T$ above 120 K. $Sr_7Mn_4O_{15}$ does not behave as a simple paramagnet above T_N, and in the absence of long-range magnetic correlations, the dc susceptibility mainly reflects the degree of short-range order in the magnetic sublattice. The ac susceptibility probes, in addition to this, also the degree of mobility of the moments in response to the oscillating magnetic field. The above mentioned spin pairing is antiferromagnetic in nature and thus gives a reduced susceptibility compared to the free ion model. With decreasing temperature the spin-spin correlations in the dimers become stronger and thus the susceptibility does not increase as much as expected on the basis of a Curie-Weiss law. This results in a dc susceptibility which can be modelled artificially by using an unreasonable large Weiss temperature. Single ion anisotropy, through spin-orbit coupling, rules that the moments have a preferential orientation along the *b* axis. In the absence of long-range magnetic order in the manganese sublattice, the influence of spin-orbit coupling increases with decreasing temperature and the paired magnetic moments ''freeze'' into the lattice leading to a decrease of χ_{ac}. As discussed above, cluster formation starts at ~150 K and on further cooling, these clusters grow in number and size, leading to a decreasing slope of the χ_{dc} and eventually to a maximum at ~100 K. Around this temperature the magnetic susceptibility is dominated by those clusters and the influence of paramagnetic uncoupled Mn ions becomes very small. At even lower temperatures the number of clusters decreases while they continue to grow in size. Since the intradimer Mn-Mn interactions remain the dominant magnetic force, χ_{ac} continues to decrease with decreasing temperature in this temperature region. At the Néel temperature (75 K) the clusters have grown large enough to allow the development of long range magnetic order and both magnetic susceptibilities start showing a similar temperature behavior. The maximum in $\partial\chi_{ac}/\partial T$ coincides with the temperature at which we observe the onset of long range ordering, and is likely to be related to this effect.

A confirmation of this hypothesis can be found in the development of the Mn(1)-Mn(2) intradimer distance with temperature. This bond length increases on cooling through the Néel temperature [Fig. 9(a)] despite the fact that Mn(1) and Mn(2) are coupled antiferromagnetically. Exchange striction effects would favor a reduction of the bond length under these conditions, as is most clearly observed for the interdimer Mn(1)-Mn(2) distance [Fig. 9(b)]. The only reasonable explanation is that the intradimer bond length is already reduced due to intradimer spin coupling. Below T_N, a compromise has to be achieved between the competing interactions, and as a result the intradimer Mn(1)-Mn(2) distance is somewhat enlarged, in favor of the interdimer distances. This effect is so strong that the intradimer Mn-Mn distance actually becomes larger than that at room temperature. Interestingly, the 180° Mn(1)-O(6)-Mn(1) bond length is also increased on the transition [Fig. 9(c)]. Apparently, the exchange striction of the relatively long Mn(1)-O(6)-Mn(1)

distance (3.77 Å at 290 K) is too weak to compete effectively with that of the shorter Mn(1)-O(5)-Mn(2) bond (3.65 Å at 290 K). This effect is likely to be even more strengthened by the two following independent factors. First, the Mn(1)-O(2)-Mn(2) bond makes an angle of ~65° with the direction of the magnetic moment, where as this angle is ~30° for the Mn(1)-O(6)-Mn(1) bond, rendering a stronger attractive force for the former. Secondly, the Mn(1)-Mn(2) interaction is twice as abundance as the Mn(1)-Mn(1). It is very hard to assess the influence of the disorder of O(6) through the Mn(1)-O(6)-Mn(1) bond angle on this force.

Returning to the low-temperature magnetic susceptibility data; we can only speculate about the origin of the upturn below ~25 K observed in both dc and ac data sets. A similar behavior was found in the dc susceptibility of other batches of $Sr_7Mn_4O_{15}$ and in that of all other $Sr_{7-x}(Ca/Ba)_xMn_4O_{15}$ compounds.[21] The fact that the upturn is always present indicates that it is likely to be an inherent effect and not due to an impurity. One of the possible causes might be intrinsic crystallographic errors resulting in dangling ends, or manganese ions in individual octahedra, which remain paramagnetic down to the lowest temperatures. Another explanation for the upturn could be a reentrance of spin-glass-like behavior as discussed earlier. More studies are required to clarify the nature of this feature.

CONCLUSION

With the discussion in mind we can now describe the magnetic properties of $Sr_7Mn_4O_{15}$ as a function of temperature. At temperatures close to room temperature, a high degree of spin pairing within the manganese dimers is present, but it is unlikely to be complete. We thus to not observe a sharp transition from a truly paramagnetic to a spin paired state as observed for $SrMnO_3$ at 350 K.[14,29] On cooling short range correlations become more and more important, and antiferroamgnetic clusters start to form at ~150 K. Those clusters can be low dimensional because of the layered nature of this compound and they start to dominate the susceptibility at ~100 K. Below this temperature, three dimensional long-range correlation start to form resulting in a reduction of the susceptibility and background level in the PND experiments. Long-range antiferromagnetic order is finally established at ~75 K.

ACKNOWLEDGMENTS

We are grateful to Ken Anderson (ISIS, Rutherford Lab), Alberto Vega (CINVESTAV), Satish Tiwary (The University of Edinburgh), and Martin R. Lees (University of Warwick, UK) for experimental assistance. This work was financially supported by the CONACyT (Grant No. 33171-E, JFV) and by the EPSRC (Grant No. GR/M75471, KVK).

*Authors to whom correspondence should be addressed. E-mail addresses: jaap@mda.cinvestav.mx (J.F.V.), kvk@ph.ed.ac.uk (K.V.K).

[1] Y. Moritomo, A. Asamitsu, H. Kuwahara, and Y. Tokura, Nature (London) **380**, 141 (1996).

[2] P. D. Battle, D. E. Cox, M. A. Green, J. E. Millburn, L. E. Spring, P. G. Radaelli, M. J. Rosseinsky, and J. F. Vente, Chem. Mater. **9**, 1042 (1997).

[3] P. D. Battle, M. A. Green, N. S. Laskey, J. E. Millburn, P. G. Radaelli, M. J. Rosseinsky, S. P. Sullivan, and J. F. Vente, Phys. Rev. B **54**, 15 967 (1996).

[4] P. D. Battle, M. A. Green, N. S. Laskey, N. Kasmir, J. E. Millburn, L. E. Spring, S. P. Sullivan, M. J. Rosseinsky, and J. F. Vente, J. Mater. Chem. **7**, 977 (1997).

[5] P. D. Battle, J. E. Millburn, M. J. Rosseinsky, L. E. Spring, J. F. Vente, and P. G. Radaelli, Chem. Mater. **9**, 3136 (1997).

[6] P. D. Battle, S. J. Blundell, M. A. Green, W. Hayes, M. Honold, A. K. Klehe, N. S. Laskey, J. E. Millburn, L. Murphy, M. J. Rosseinsky, N. A. Samarin, J. Singleton, N. A. Sluchanko, S. P. Sullivan, and J. F. Vente, J. Phys.: Condens. Matter **8**, L427 (1996).

[7] A. I. Coldea, L. E. Spring, S. J. Blundell, J. Singleton, and W. Hayes, J. Phys.: Condens. Matter **11**, 9053 (1999).

[8] Y. Shimakawa, Y. Kubo, and T. Manako, Nature (London) **379**, 53 (1996).

[9] A. I. Mihut, L. E. Spring, R. I. Bewley, S. J. Blundell, W. Hayes, T. Jestädt, B. W. Lovett, R. McDonald, F. L. Pratt, J. Singleton, P. D. Battle, J. Lago, M. J. Rosseinsky, and J. F. Vente, J. Phys.: Condens. Matter **10**, L727 (1998).

[10] J. B. Goodenough, *Magnetism and the Chemical Bond* (Wiley, New York, 1963).

[11] C. N. R. Rao, A. K. Cheetham, and R. Mahesh, Chem. Mater. **8**, 2421 (1996).

[12] J. F. Vente, J. R. Plaisier, D. J. W. IJdo, and K. V. Kamenev, Mater. Res. Bull. **35**, 2437 (2000).

[13] R. Kriegel, A. Feltz, L. Walz, A. Simon, and H. J. Mattausch, Z. Anorg. Allg. Chem. **617**, 99 (1992).

[14] P. D. Battle, T. C. Gibb, and C. W. Jones, J. Solid State Chem. **74**, 60 (1988).

[15] J. C. Bouloux, J. L. Soubeyroux, G. le-Flem, and P. Hagenmüller, J. Solid State Chem. **38**, 34 (1981).

[16] A. Feltz, R. Kriegel, and W. Pölzl, J. Mater. Sci. Lett. **18**, 1693 (1999).

[17] H. M. Rietveld, J. Appl. Crystallogr. **2**, 65 (1969).

[18] A. C. Larson and R. B. von-Dreele, *General Structure Analysis System* (GSAS), Los Alamos National Laboratory.

[19] W. I. F. David, J. Appl. Crystallogr. **19**, 63 (1986).

[20] A. W. Hewat, Acta Crystallogr., Sect. A: Cryst. Phys., Diffr., Theor. Gen. Crystallogr. **35**, 248 (1979).

[21] J. F. Vente (unpublished).

[22] S. Greenwald and J. S. Smart, Nature (London) **166**, 523 (1950).

[23] P. D. Battle, M. A. Green, J. Lago, J. E. Millburn, M. J. Rosseinsky, and J. F. Vente, Chem. Mater. **10**, 658 (1998).

[24] K. Tezuka, M. Inamura, and Y. Hinatsu, J. Solid State Chem. **145**, 705 (1999).

[25] J. Fábry, J. Hybler, Z. Jirak, K. Jurek, K. Maly, M. Nevriva, and

V. Petricek, J. Solid State Chem. **73**, 520 (1988).
[26] E. J. Cussen and P. D. Battle, Chem. Mater. **12**, 831 (2000).
[27] I. D. Brown and D. Altermatt, Acta Crystallogr., Sect. B: Struct. Sci. **41**, 244 (1985).
[28] E. J. Cussen, J. Sloan, J. F. Vente, P. D. Battle, and T. C. Gibb, Inorg. Chem. **37**, 6071 (1998).
[29] B. L. Chamberland, A. W. Sleight, and J. F. Weiher, J. Solid State Chem. **1**, 506 (1970).